

Pseudo magnetic field in strained graphene: revisited

M. Ramezani Masir, D. Moldovan, F. M. Peeters

*Departement Fysica, Universiteit Antwerpen
Groenenborgerlaan 171, B-2020 Antwerpen, Belgium.*

Abstract

We revisit the theory of the pseudo magnetic field as induced by strain in graphene using the tight-binding approach. A systematic expansion of the hopping parameter and the deformation of the lattice vectors is presented from which we obtain an expression for the pseudo magnetic field for low energy electrons. We generalize and discuss previous results and propose a novel effective Hamiltonian. The contributions of the different terms to the pseudo magnetic field expression is investigated for a model triaxial strain profile and are compared with the full solution. Our work suggests that the previous proposed pseudo magnetic field expression is valid up to reasonably high strain (15%) and there is no \mathbf{K} -dependent pseudo-magnetic field.

Keywords: Graphene; Effective Hamiltonian; Strain; Pseudo magnetic field

1. Introduction

Graphene has triggered a broad activity both in fundamental and applied physics and chemistry. The most intriguing feature of this system is their similarity to ultrarelativistic electrons and positrons obeying the Dirac equation [1, 2]. An interesting prediction is that a geometrical deformation of the graphene lattice results in a local strain that acts as a pseudo-magnetic field on the electronic degrees of freedom and which leads to a pseudo-quantum Hall effect [3]. Graphene can sustain very high, up to 25%, elastic strains [4] which leads to a shift in the position of the Dirac cones [5]. Deformation due to elastic strain changes the hopping amplitude of the carbon atoms and induces an effective vector potential that shifts the Dirac point [7]. With a proper geometrical deformation it is possible to create large pseudo-magnetic fields of different shapes [3, 8, 9]. It has been predicted that applying strain with triangular symmetry results in an uniform pseudo-magnetic field of the order of 10T [6]. Recently it was reported experimentally [11] that nanobubbles grown on a Pt(111) surface induce pseudo-magnetic fields of more than 300 T. Landau quantization of the electronic spectrum was observed by scanning tunneling microscopy. Thus strain engineering has become a new way to control the electronic properties of graphene [9, 10].

The effective vector potential induced by strain was derived in Refs. [13, 14] and was based on a tight binding approach with the important approximation that the local strain does not alter the lattice vectors. Very recently it was shown that including the deformation of the lattice vectors leads to an extra term for the effective magnetic field which is of the same order of magnitude and which differ in the different K points [15]. But later it was shown that this extra term in the

effective vector potential does not have any contribution to the induced pseudo magnetic field [16] and that subsequently there is no difference in the different \mathbf{K} -points. Furthermore, in Ref. [17, 18] it is shown that in the presence of strain the Fermi velocity becomes spatial dependent.

In this manuscript we revisit the problem and present a systematic study of the different corrections to the vector potential and compare them with the numerically obtained full pseudo magnetic field. We present the effective Hamiltonian that includes different contributions of strain. The previous result for the vector potential and the Fermi velocity reobtained in our systematic expansion. As an example we present explicit analytical results for strained graphene as induced by a uniaxial and triaxial strain. We find the magnetic field induced by the in-plane deformation and compared the different terms for the vector potential [13, 14, 15] with the exact numerical results for the pseudo magnetic field.

2. Strain Field

The Hamiltonian in the tight-binding approximation considering only the first nearest neighbor is given by:

$$H = - \sum_{i,j} t_0 a_i^\dagger b_j + h.c., \quad (1)$$

where t_0 is the hopping parameter and a_i and a_i^\dagger (b_i and b_i^\dagger) are the annihilation and creation operator for an electron on sublattice A (B). In the presence of lattice deformation the hopping parameter t changes due to the changing interatomic distance. The modification of the hopping parameter due to strain is given by [5],

$$t_n = t_0 e^{-\beta(d_n/a-1)}, \quad (2)$$

where a is the unstrained nearest neighbor distance, $\beta \approx 2 - 3.37$ and d_n is the length of the

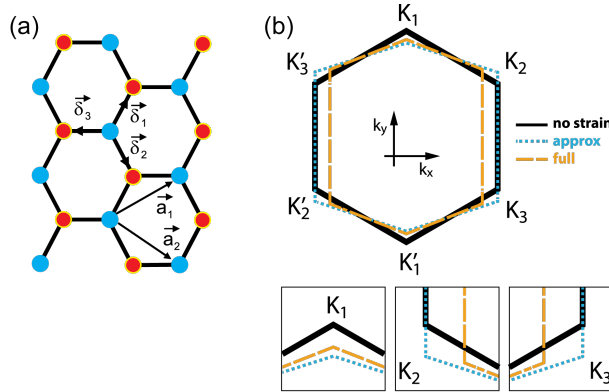


Figure 1: (a) A monolayer graphene lattice, $\mathbf{a}_1 = (3/2, \sqrt{3}/2)a$ and $\mathbf{a}_2 = (3/2, -\sqrt{3}/2)a$ are the basis vectors and the sublattices are connected by $\delta_1 = (1/2, \sqrt{3}/2)a$, $\delta_2 = (1/2, -\sqrt{3}/2)a$ and $\delta_3 = (-1, 0)a$. (b) The normal (solid black line) and deformed (yellow dashed line for full solution and blue dotted for approximated pseudo magnetic field) Brillouin zone with \mathbf{K} points given by $\mathbf{K}_1 = \frac{4\pi}{3\sqrt{3}a} (0, 1)$, $\mathbf{K}_2 = \frac{2\pi}{3\sqrt{3}a} (\sqrt{3}, -1)$ and $\mathbf{K}_3 = \frac{2\pi}{3\sqrt{3}a} (-\sqrt{3}, -1)$.

strained lattice vector. Using the Fourier transform of the creation and annihilation operators we

obtain the strained Hamiltonian as:

$$H = - \sum_{n,\mathbf{k}} t_n e^{-i\mathbf{k}\cdot\mathbf{d}_n} a_{\mathbf{k}}^\dagger b_{\mathbf{k}} + H.c. \quad (3)$$

$\mathbf{d}_n = (\bar{I} + \bar{u})\delta_n$, where \bar{I} is the unity matrix and \bar{u} is the strain tensor. The strain elements of the tensor are given by [18, 16], $\bar{u} = \bar{\epsilon} + \bar{\omega}$, and it consists of two parts: the linear part of strain tensor given by,

$$\bar{\epsilon}_{ij} = \frac{1}{2} \left\{ \frac{\partial u_i}{\partial x_j} + \frac{\partial u_j}{\partial x_i} \right\}. \quad (4)$$

and the rotational part $\bar{\omega}$ given by

$$\bar{\omega}_{ij} = \frac{1}{2} \left\{ \frac{\partial u_i}{\partial x_j} - \frac{\partial u_j}{\partial x_i} \right\}. \quad (5)$$

On the other hand we can obtain the change in the lattice vectors size as

$$\begin{aligned} d\ell'^2 &= dx'_i dx'_i = dx_i dx_i + 2du_i dx_i + du_i du_i \\ &= d\ell^2 + 2 \frac{du_i}{dx_k} dx_i dx_k + \frac{du_l}{dx_k} \frac{du_l}{dx_k} dx_i dx_k \\ &= d\ell^2 + 2 \left\{ \underbrace{\frac{1}{2} \left(\frac{du_i}{dx_k} + \frac{du_k}{dx_i} \right) dx_i dx_k}_1 + \underbrace{\frac{1}{2} \left(\frac{du_i}{dx_k} - \frac{du_k}{dx_i} \right) dx_i dx_k}_2 \right\} + \frac{du_l}{dx_k} \frac{du_l}{dx_k} dx_i dx_k \\ &= d\ell^2 + 2 \left\{ \bar{\epsilon}_{ij} dx_i dx_k + \bar{\omega}_{ij} dx_i dx_k \right\} + \frac{du_l}{dx_k} \frac{du_l}{dx_k} dx_i dx_k. \end{aligned} \quad (6)$$

The first symmetric term denoted by 1 correspond with the linear part of the strain and the second term denoted by 2 correspond with rotational tensor and has zero contribution to the nearest neighbor vector sizes. The hopping changes with carbon-carbon distance but the rotational tensor term does not contribute to it.

First we drive the effective Hamiltonian by expanding Eq. (3) up to the first order in strain [15] (The second order terms are included in the subsequent discussion but are not listed in the expansion of the Hamiltonian because of those expressions are rather involved),

$$\begin{aligned} H &= - \sum_{n=1}^3 t_n \begin{pmatrix} 0 & e^{-i(\mathbf{K}+\mathbf{q})\cdot\mathbf{d}_n} \\ e^{i(\mathbf{K}+\mathbf{q})\cdot\mathbf{d}_n} & 0 \end{pmatrix} \\ &\approx - \sum_{n=1}^3 t_n \begin{pmatrix} 0 & e^{-i\mathbf{K}\cdot\mathbf{a}_n} \\ e^{i\mathbf{K}\cdot\mathbf{a}_n} & 0 \end{pmatrix} (1 + i\sigma_z \mathbf{K} \cdot \bar{u} \mathbf{a}_n) (1 + i\sigma_z \mathbf{q} \cdot \mathbf{d}_n) \\ &= - \sum_{n=1}^3 t_0 \left(1 - \frac{\beta}{a^2} \mathbf{a}_n \cdot \bar{u} \cdot \mathbf{a}_n \right) \left(\frac{i}{a} (\boldsymbol{\sigma} \cdot \mathbf{a}_n) \sigma_z \right) (1 + i\sigma_z \mathbf{K} \cdot \bar{u} \mathbf{a}_n) \\ &\quad \times (1 + i\sigma_z \mathbf{q} \cdot \mathbf{a}_n + i\sigma_z \mathbf{q} \cdot \bar{u} \mathbf{a}_n). \end{aligned} \quad (7)$$

The different terms of the effective Hamiltonian are shown in Table. 1. The first term is the

famous Dirac-Weyl equation,

$$\begin{aligned} H_0 &= - \sum_{n=1}^3 t_0 \left(\frac{i}{a} (\boldsymbol{\sigma} \cdot \mathbf{a}_n) \sigma_z \right) (i\sigma_z \mathbf{q} \cdot \mathbf{a}_n) = v_0 \boldsymbol{\sigma} \cdot \mathbf{p}, \\ H_0 &= -i\hbar v_0 \boldsymbol{\sigma} \cdot \boldsymbol{\nabla} \end{aligned} \quad (8)$$

There are three terms in the first order of strain,

$$\begin{aligned} H_1 &= \sum_{n=1}^3 t_0 \left(\frac{1}{a} (\boldsymbol{\sigma} \cdot \mathbf{a}_n) \sigma_z \right) (\sigma_z \mathbf{q} \cdot \bar{u} \mathbf{a}_n) = v_0 \boldsymbol{\sigma} \cdot \bar{u} \cdot \mathbf{p}, \\ H_1 &= -i\hbar v_0 \left(\boldsymbol{\sigma} \cdot \bar{u} \cdot \boldsymbol{\nabla} + \frac{1}{2} \boldsymbol{\sigma} \cdot \boldsymbol{\nabla}^T \cdot \bar{u} \right) \end{aligned} \quad (9)$$

the second term is β -dependent and is given by

$$\begin{aligned} H_2 &= \sum_{n=1}^3 t_0 \left(\frac{\beta}{a^2} \mathbf{a}_n \cdot \bar{u} \cdot \mathbf{a}_n \right) \left(\frac{1}{a} (\boldsymbol{\sigma} \cdot \mathbf{a}_n) \sigma_z \right) (\sigma_z \mathbf{q} \cdot \mathbf{a}_n) \\ &= \frac{\beta v_F}{4} \boldsymbol{\sigma} \cdot (2\bar{u} + Tr(u)\bar{I}) \cdot \mathbf{p}, \end{aligned} \quad (10)$$

$$H_2 = -i\hbar \frac{\beta v_F}{4} \boldsymbol{\sigma} \cdot \left(2\bar{u} \cdot \boldsymbol{\nabla} + Tr(u)\bar{I} \cdot \boldsymbol{\nabla} + \boldsymbol{\nabla}^T \cdot \bar{u} + \frac{1}{2} \boldsymbol{\nabla}^T \cdot Tr(u)\bar{I} \right)$$

and is the same as the term introduced in Refs. [17, 18]. The third and last term is β -independent and is given by

$$\begin{aligned} H_3 &= - \sum_{n=1}^3 t_0 \left(\frac{i}{a} (\boldsymbol{\sigma} \cdot \mathbf{a}_n) \sigma_z \right) (i\sigma_z \mathbf{K} \cdot \bar{u} \mathbf{a}_n) (i\sigma_z \mathbf{q} \cdot \mathbf{a}_n) \\ &= i \frac{v_F^0 a}{2} \boldsymbol{\sigma} \cdot (\mathbf{K} \cdot \bar{u} \cdot \boldsymbol{\omega}) \cdot \mathbf{p} \\ H_3 &= \hbar \frac{v_F^0 a}{2} \boldsymbol{\sigma} \cdot \left\{ (\mathbf{K} \cdot \bar{u} \cdot \boldsymbol{\omega}) \cdot \boldsymbol{\nabla} + \frac{1}{2} \boldsymbol{\nabla} \cdot (\mathbf{K} \cdot \bar{u} \cdot \boldsymbol{\omega}) \right\} \end{aligned} \quad (11)$$

Here $v_F^0 = 3ta/2\hbar$, $\boldsymbol{\sigma} = (\sigma_x, \sigma_y)$ are the Pauli matrices, and $\boldsymbol{\omega} = (-\sigma_z, \sigma_x)$. In summary we can write the full effective Hamiltonian up to the first order in strain, considering both the β -dependent and β -independent terms as

$$H_{eff} = H_0 + H_1 + H_2 + H_3. \quad (12)$$

Now the β -dependent Fermi velocity is replaced by a tensor,

$$\bar{v}_F = v_F^0 \left(\bar{I} + \frac{\beta}{4} [2\bar{u} + Tr(u)\bar{I}] \right) \quad (13)$$

which is space-dependent [17, 18].

Next we derive the pseudo magnetic field induced by strain. The pseudo-magnetic vector potential $A_{ps} = A_x + iA_y$ induced by strain is given by [5],

$$A_{ps} = \frac{1}{e v_F} \sum_n^3 t_n e^{-i\mathbf{K} \cdot \mathbf{d}_n}, \quad (14)$$

Table 1: Different terms induced by strain in the expansion of the vector potential. Right column indicates the order of these terms in the strain (i. e. $O(u^2)$) and their effect on the different properties.

n	Expansion terms	
1	$e^{-i\mathbf{K}\cdot\delta_n}$	0
2	$-i\mathbf{q}\cdot\delta_n e^{-i\mathbf{K}\cdot\delta_n}$	Dirac equation
3	$-i\mathbf{q}\cdot\bar{\mathbf{u}}\cdot\delta_n e^{-i\mathbf{K}\cdot\delta_n}$	v_F β -independent
4	$-\frac{\beta}{a^2}(\delta_n\cdot\bar{\mathbf{u}}\cdot\delta_n) e^{-i\mathbf{K}\cdot\delta_n}$	Effective vector potential A_0
5	$\frac{i\beta}{a^2}(\delta_n\cdot\bar{\mathbf{u}}\cdot\delta_n)(\mathbf{q}\cdot\mathbf{a}_n) e^{-i\mathbf{K}\cdot\delta_n}$	Fermi velocity v_F β -dependent $O(1)$
6	$\frac{i\beta}{a^2}(\delta_n\cdot\bar{\mathbf{u}}\cdot\delta_n)(\mathbf{q}\cdot\bar{\mathbf{u}}\cdot\delta_n) e^{-i\mathbf{K}\cdot\delta_n}$	Fermi velocity v_F β -dependent $O(2)$
7	$-i(\mathbf{K}\cdot\bar{\mathbf{u}}\cdot\delta_n) e^{-i\mathbf{K}\cdot\delta_n}$	Effective \mathbf{A} β -independent $O(1)$
8	$\frac{i\beta}{a^2}(\delta_n\cdot\bar{\mathbf{u}}\cdot\delta_n)(\mathbf{K}\cdot\bar{\mathbf{u}}\cdot\delta_n) e^{-i\mathbf{K}\cdot\delta_n}$	Effective \mathbf{A} β -dependent $O(2)$
9	$\frac{\beta^2}{2a^4}(\delta_n\cdot\bar{\mathbf{u}}\cdot\delta_n)^2 e^{-i\mathbf{K}\cdot\delta_n}$	Effective \mathbf{A} β -dependent $O(2)$
10	$-\frac{1}{2}(\mathbf{K}\cdot\bar{\mathbf{u}}\cdot\delta_n)^2 e^{-i\mathbf{K}\cdot\delta_n}$	Effective \mathbf{A} β -independent $O(2)$
11	$-(\mathbf{K}\cdot\bar{\mathbf{u}}\cdot\delta_n)(\mathbf{q}\cdot\delta_n) e^{-i\mathbf{K}\cdot\delta_n}$	v_F β -independent $O(1)$
12	$-(\mathbf{K}\cdot\bar{\mathbf{u}}\cdot\delta_n)(\mathbf{q}\cdot\bar{\mathbf{u}}\cdot\delta_n) e^{-i\mathbf{K}\cdot\delta_n}$	v_F β -independent $O(2)$
13	$\frac{\beta}{a^2}(\delta_n\cdot\bar{\mathbf{u}}\cdot\delta_n)(\mathbf{K}\cdot\bar{\mathbf{u}}\cdot\delta_n)(\mathbf{q}\cdot\delta_n) e^{-i\mathbf{K}\cdot\delta_n}$	v_F β -dependent $O(2)$
14	$-\frac{\beta^2}{2a^4}(\delta_n\cdot\bar{\mathbf{u}}\cdot\delta_n)^2(\mathbf{q}\cdot\delta_n) e^{-i\mathbf{K}\cdot\delta_n}$	v_F β -dependent $O(2)$

where v_F is the Fermi velocity, t_n are the strained nearest-neighbor hopping parameters. Note that A_{ps} is imaginary because strain breaks inversion symmetry in the nearest neighbor hopping. The effective pseudo magnetic field induced by strain will shift the \mathbf{K} -points as $\mathbf{K}_n \rightarrow \mathbf{K}_n + \mathbf{A}_n$ (see Fig. 1(b)). Writing the wave vector \mathbf{k} with respect to the Dirac cone using $\mathbf{k} = \mathbf{K} + \mathbf{q}$ and expanding the exponent and hopping parameter t_n up to second order we find:

$$t_0 \left(1 + \delta t_n + \frac{1}{2} \delta t_n^2 \right) \left(1 - i\mathbf{K}\cdot\bar{\mathbf{u}}\cdot\delta_n - \frac{1}{2}(\mathbf{K}\cdot\bar{\mathbf{u}}\cdot\delta_n)^2 \right) \times (1 - i\mathbf{q}\cdot\delta_n - i\mathbf{q}\cdot\bar{\mathbf{u}}\cdot\delta_n) e^{-i\mathbf{K}\cdot\delta_n} \quad (15)$$

where $\delta t = -\frac{\beta}{a^2} \delta_n\cdot\bar{\mathbf{u}}\cdot\delta_n$. The effective vector potential is given by \mathbf{q} independent terms. Keeping the hopping parameters up to second order and expanding $e^{-i\mathbf{K}\cdot\delta_n}$ we find

$$t_n e^{-i\mathbf{K}\cdot\delta_n} \approx t_0 \left\{ 1 + \underbrace{\delta t_n}_1 - \underbrace{i\mathbf{K}\cdot\bar{\mathbf{u}}\cdot\delta_n}_2 \right. \\ \left. - \underbrace{i\delta t_n \mathbf{K}\cdot\bar{\mathbf{u}}\cdot\delta_n - \frac{1}{2}(\mathbf{K}\cdot\bar{\mathbf{u}}\cdot\delta_n)^2 + \frac{1}{2}\delta t_n^2}_3 \right\} e^{-i\mathbf{K}\cdot\delta_n} \quad (16)$$

The first correction term is the one obtained in Refs. [13, 14] and the second correction term was recently added by Kit *et al.* [15]. The third term is the new higher order correction term which we will add.

Considering only the first term we take constant lattice vectors $\mathbf{d}_n = \delta_n$. Using the three nearest neighbors vectors in real space (as shown in Fig. 1) $\delta_1 = \frac{a}{2}(1, \sqrt{3})$, $\delta_2 = \frac{a}{2}(1, -\sqrt{3})$, $\delta_3 = a(-1, 0)$ and the position of the \mathbf{K} -points are given by $\mathbf{K}_1 = \frac{4\pi}{3\sqrt{3}a}(0, 1)$, $\mathbf{K}_2 = \frac{2\pi}{3\sqrt{3}a}(\sqrt{3}, -1)$ and $\mathbf{K}_3 = \frac{2\pi}{3\sqrt{3}a}(-\sqrt{3}, -1)$ we obtain the vector potential in terms of the strain tensor elements,

$$\mathbf{A}_1 = \frac{\phi_0\beta}{4\pi a} \begin{pmatrix} u_{xx} - u_{yy} \\ 2u_{xy} \end{pmatrix} \quad (17)$$

where $\phi_0 = h/e$ is the flux quantum.

In order to obtain the correction given in Ref. [15] we need to include the change of the lattice vectors with deformation as $\mathbf{d}_n = (\bar{I} + \bar{u})\delta_n$. Including this correction we find the following extra term to the vector potential for the different \mathbf{K} -points,

$$\begin{aligned} \mathbf{A}_2^{K_1} &= \frac{\phi_0}{2a} \frac{4}{3\sqrt{3}} \begin{pmatrix} u_{yy} \\ u_{xy} \end{pmatrix}, \\ \mathbf{A}_2^{K_2} &= \frac{\phi_0}{2a} \begin{pmatrix} \frac{2}{3}u_{xy} - \frac{2\sqrt{3}}{9}u_{yy} \\ \frac{2}{3}u_{xx} - \frac{2\sqrt{3}}{9}u_{xy} \end{pmatrix}, \\ \mathbf{A}_2^{K_3} &= \frac{\phi_0}{2a} \begin{pmatrix} -\frac{2}{3}u_{xy} - \frac{2\sqrt{3}}{9}u_{yy} \\ -\frac{2}{3}u_{xx} - \frac{2\sqrt{3}}{9}u_{xy} \end{pmatrix}. \end{aligned} \quad (18)$$

It is possible to show that this effective vector potential has the form of $\nabla\chi$. We start with

$$\begin{aligned} A_2 &= -\frac{3t_0a}{2} \{\mathbf{K} \cdot \bar{\mathbf{u}} \cdot \mathbf{s}\} \\ &= -\frac{3t_0a}{2} \sum_{i,j} \{K_i \bar{u}_{ij} s_j\} \\ &= -\frac{3t_0a}{2} \sum_{i,j} K_i \left(\frac{\partial u_i}{\partial x_j} \right) s_j \\ &= -\frac{3t_0a}{2} \nabla(\mathbf{K} \cdot \mathbf{u}) \cdot \mathbf{s} \end{aligned} \quad (19)$$

and the two components of the vector potential is given by the real and complex part of \mathbf{A}_2 as

$$\begin{aligned} A_x &\propto \partial_x (\mathbf{K} \cdot \mathbf{u}) \\ A_y &\propto \partial_y (\mathbf{K} \cdot \mathbf{u}) \end{aligned} \quad (20)$$

and the magnetic field is given by $\mathbf{B}_2 = \nabla \times \mathbf{A}_2 = 0$, which shows that there is no \mathbf{K} -dependent pseudo-magnetic fields.

Next we include the second order strain part and try to find effective vector potential,

$$\mathbf{A}_3^{\mathbf{K}} = \underbrace{-i\delta t_n \mathbf{K} \cdot \bar{\mathbf{u}} \cdot \delta_n}_{I_1} + \underbrace{\frac{1}{2}\delta t_n^2}_{I_2} - \underbrace{\frac{t_0}{2}(\mathbf{K} \cdot \bar{\mathbf{u}} \cdot \delta_n)^2}_{I_3}, \quad (21)$$

and the corresponding vector potential for the different \mathbf{K} -points is given by

$$\begin{aligned}
I_1^{K_1} &= \frac{\phi_0}{2a} \begin{pmatrix} -\frac{\beta}{3\sqrt{3}}(u_{xx}u_{yy} + 3u_{yy}^2 + 2u_{xy}^2) \\ \frac{\beta}{\sqrt{3}}(u_{xx}u_{xy} + u_{xy}u_{yy}) \end{pmatrix}, \\
I_1^{K_2} &= \frac{\phi_0}{2a} \frac{\beta}{3\sqrt{3}} \begin{pmatrix} -2u_{xy}^2 + 3\sqrt{3}u_{xy}u_{yy} + 3\sqrt{3}u_{xx}u_{xy} - 3u_{yy}^2 - u_{xx}u_{yy} \\ -3\sqrt{3}u_{xx}^2 + 3u_{xx}u_{xy} - \sqrt{3}u_{yy}u_{xx} - 2\sqrt{3}u_{xy}^2 + 3u_{yy}u_{xy} \end{pmatrix}, \\
I_1^{K_3} &= \frac{\phi_0}{2a} \frac{\beta}{3\sqrt{3}} \begin{pmatrix} 2u_{xy}^2 + 3\sqrt{3}u_{xy}u_{yy} + 3\sqrt{3}u_{xx}u_{xy} + 3u_{yy}^2 + u_{xx}u_{yy} \\ -3\sqrt{3}u_{xx}^2 - 3u_{xx}u_{xy} - \sqrt{3}u_{yy}u_{xx} - 2\sqrt{3}u_{xy}^2 - 3u_{yy}u_{xy} \end{pmatrix}.
\end{aligned} \tag{22}$$

The correction corresponding to $\delta t^2/2$ is given by

$$I_2^K = \frac{1}{2} \delta t^2 \rightarrow \frac{\phi_0}{2a} \begin{pmatrix} \frac{\beta^2}{8\pi}(5u_{xx}^2 - 2u_{xx}u_{yy} - 4u_{xy}^2 - 3u_{yy}^2) \\ -\frac{3\beta^2}{2\pi}u_{xy}(u_{xx} + 3u_{yy}) \end{pmatrix} \tag{23}$$

and the vector potential resulting from the last contribution $-\frac{t_0}{2}(\mathbf{K} \cdot \bar{\mathbf{u}} \cdot \delta_n)^2$ in the different \mathbf{K} -points is given by,

$$\begin{aligned}
I_3^{K_1} &= \frac{\phi_0}{3a} \frac{4\pi}{9} \begin{pmatrix} u_{xy}^2 - u_{yy}^2 \\ -2u_{xy}u_{yy} \end{pmatrix}, \\
I_3^{K_2} &= \frac{\phi_0}{3a} \frac{4\pi}{9} \begin{pmatrix} 3u_{xx}^2 - 2u_{xy}^2 - u_{yy}^2 + 2\sqrt{3}u_{xy}(u_{yy} - u_{xx}) \\ -2(u_{xy} - \sqrt{3}u_{xx})(u_{yy} - \sqrt{3}u_{xy}) \end{pmatrix}, \\
I_3^{K_3} &= \frac{\phi_0}{3a} \frac{4\pi}{9} \begin{pmatrix} 3u_{xx}^2 - 2u_{xy}^2 - u_{yy}^2 + 2\sqrt{3}u_{xy}(u_{xx} - u_{yy}) \\ -2(u_{xy} + \sqrt{3}u_{xx})(u_{yy} + \sqrt{3}u_{xy}) \end{pmatrix}.
\end{aligned} \tag{24}$$

This correction is of second order in the strain and is thus important for large strains and the corresponding effective field is position dependent. The most important term is $I_2 = \frac{1}{2} \delta t^2$ which is \mathbf{K} -independent and it is possible to show that the two other terms I_1 and I_3 have a non-zero contribution to the vector potential but have zero contribution in pseudo-magnetic field.

3. Fermi velocity for uniaxial strain

The tight-binding Hamiltonian for an infinite sheet of graphene is given by,

$$H = \begin{pmatrix} 0 & f(\mathbf{k}) \\ f^*(\mathbf{k}) & 0 \end{pmatrix} \tag{25}$$

where,

$$f(\mathbf{k}) = \sum_{n=1}^3 t_n e^{i\mathbf{k} \cdot \mathbf{d}_n}. \tag{26}$$

Here, t_n is the strained hopping parameter which is given by[17],

$$t_n = t_0 e^{-\beta \omega_n} \tag{27}$$

where $\omega_n = l_n/a_{cc} - 1$. Here $t_0 = -2.8$ eV is the unstrained hopping parameter, l_n is the strained distance to the nearest neighbor atom n , $a_{cc} = 0.142$ nm is the unstrained carbon-carbon distance and $\beta = 3.37$ is the strained hopping energy modulation factor. The strained nearest-neighbor vectors are given by $\mathbf{d}_n = (1 + \bar{u})\delta_n$.

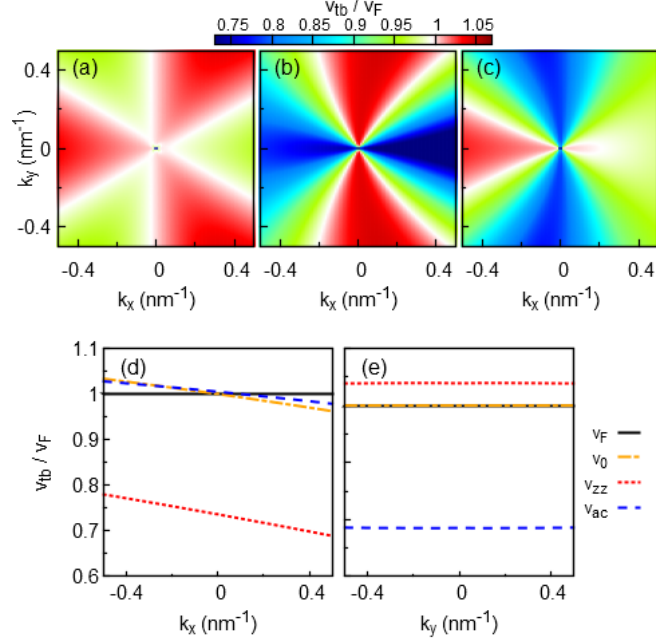


Figure 2: Top: Contour plots of v_{tb}/v_F near the Dirac point for: (a) v_0 unstrained graphene, (b) v_{zz} uniaxial zigzag strain and (c) v_{ac} uniaxial armchair strain. Bottom: Fermi velocity along the cuts where (d) $k_y = 0$ and (e) $k_x = 0$, for all three cases of the velocity: v_0 , v_{zz} and v_{ac} . The solid black line indicates the traditional continuum limit Fermi velocity v_F . The strain intensity is 10%.

We calculate the energy spectrum $E(\mathbf{k})$ of a graphene sheet from the tight-binding Hamiltonian. The velocity can then be obtained as $\mathbf{v} = \nabla_{\mathbf{k}}E(\mathbf{k})$. We calculate the velocity for three cases: 1) unstrained graphene, 2) graphene strained in the zigzag (zz) direction and 3) graphene strained in the armchair (ac) direction. The results are shown in Fig. 2. Note that we only consider the part of the spectrum that is close to the Dirac point where the continuum limit may be applied (up to 300 meV). The velocity obtained from tight-binding is scaled by the traditional continuum limit Fermi velocity $v_F = \frac{3ta_{cc}}{2\hbar}$. In the case of unstrained graphene from Fig. 2(a), the deviation of v_{tb} from v_F is generally smaller than 3%. However, moving to strained graphene (see Figs. 2(b,c)), the velocity deviates from v_F by as much as 25%.

4. Pseudo-magnetic field for triaxial strain

The displacement of triaxial strain is given by $\mathbf{u}(\mathbf{r}) = (u_x, u_y)$,

$$\begin{aligned} u_x &= 2cxy, \\ u_y &= \frac{c}{8}(x^2 - y^2), \end{aligned} \quad (28)$$

where c is a constant. The corresponding strain tensor $u_{ij}(\mathbf{r}) = \partial_j u_i$ is,

$$\bar{u}(\mathbf{r}) = c \begin{pmatrix} y & x \\ x & -y \end{pmatrix}. \quad (29)$$

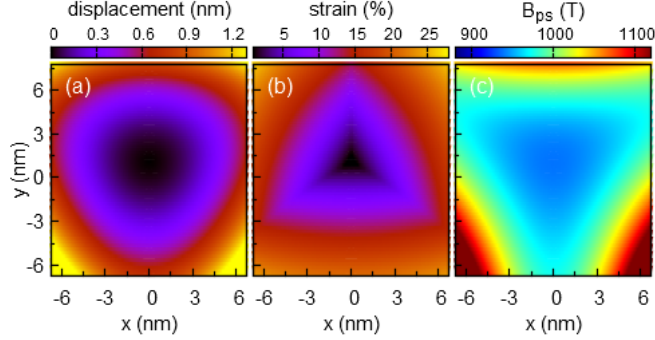


Figure 3: Contour plots of: (a) the displacement profile $|\mathbf{u}(\mathbf{r})|$ of the triaxial strain; (b) strain distribution, (c) pseudo-magnetic field calculated using the full value of the hopping parameter. The constant of the triaxial strain is: $c = 0.015 \text{ nm}^{-1}$.

The pseudo-magnetic vector potential induced by strain in graphene is given by Eq. (16), and the pseudo-magnetic field is then found as $\mathbf{B}_{ps} = \nabla \times \mathbf{A}_{ps}$. The vector potential depends on the strained hopping parameter Eq. (27), which can be expanded as,

$$t_i/t_0 = 1 + \delta t_i^{(1)} + \delta t_i^{(2)} + \delta t_i^{(3)} \dots, \quad (30)$$

$$t_i = t_0 \left(1 - \beta \omega_i + \frac{1}{2} \beta^2 \omega_i^2 - \frac{1}{6} \beta^3 \omega_i^3 \dots \right). \quad (31)$$

Usually, only the first order term $\delta t_i^{(1)}$ is taken. Here, we will evaluate the effect of the inclusion of the higher order terms.

A contour plot of the displacement profile of the triaxial strain is shown in Figs. 3(a). The pseudo-magnetic field in Fig. 3(c) is calculated using the full hopping parameter from Eq. (27). The pseudo-magnetic field is mostly homogeneous in the center. Away from the center, the magnitude of the field follows the triangular shape of the displacement with high magnitudes of the pseudo-magnetic field corresponding to locations of large displacement. In Fig. 4 we plot the pseudo-magnetic field for different approximations of the hopping parameter Eq. (30). The figures are shown in pairs, with the top ones presenting the magnitude of the field and the bottom ones presenting the difference between the approximate and the full pseudo-magnetic field calculated without approximations (see Fig. 3(d)). Taking the first order approximation, see Figs. 4(d) and (f), results in an almost completely homogeneous pseudo-magnetic field, which shows large differences compared to the full solution. Taking the second order approximation results in a less homogeneous field which, however, shows a circular symmetry instead of the triangular shape of the full field. Calculating the pseudo-magnetic field using the third order approximation finally shows the same triangular shape as the exact pseudo-magnetic field. Adding the fourth order term further improves the accuracy, but the correct shape has already been achieved with the third order approximation.

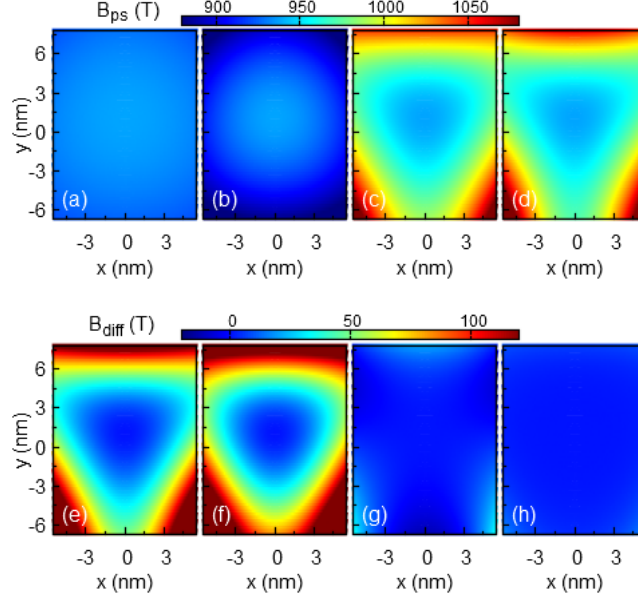


Figure 4: Top: Contour plots of the pseudo-magnetic field generated from different approximations of the hopping parameter up to: (a) first, (b) second, (c) third and (d) fourth order. Bottom: (e,f,g,h) Difference plots between the respective approximations (a,b,c,d) and the field calculated using the full value of the hopping parameter, as in Fig. 3(d). The parameters of the triaxial strain is the same as in Fig. 3.

In Fig. 5 we compare the pseudo-magnetic field approximations at three points as function of applied strain. We varied the c parameter of the triaxial strain from 0 to 0.025 nm^{-1} . The first point (A) is located in the center where the strain remains very low (below 0.5%) even for high values of c . Because of the low strain, all approximations are able to accurately estimate the field.

Next, we considered point B, where the strain reaches up to 25%. Because of the higher strain, the different approximations start to diverge, although the differences aren't very large. The different approximations diverge above 15% strain but the differences remain small even above 20%. However, point C shows more significant differences. The approximations diverge at already for 6% strain. At high strain, the first order approximation significantly underestimates the field (by as much as 350 T). Adding the second order term actually results in an even larger underestimation of the field. Finally, adding the third order term corrects the field magnitude so that it is in good agreement with the full solution.

From these results we see that a correct estimation of the field in point C is more difficult than in point B even though the maximum strain is actually lower in point C. This is because the pseudo-magnetic field depends not only on the intensity of the strain, but also on the direction. The strain in point B is mostly uniaxial, as it lies exactly along one of the three strain directions (see Fig. 5(a)). On the other hand, point B feels a strong influence from both of the top strain directions, so it is strongly non-uniaxial.

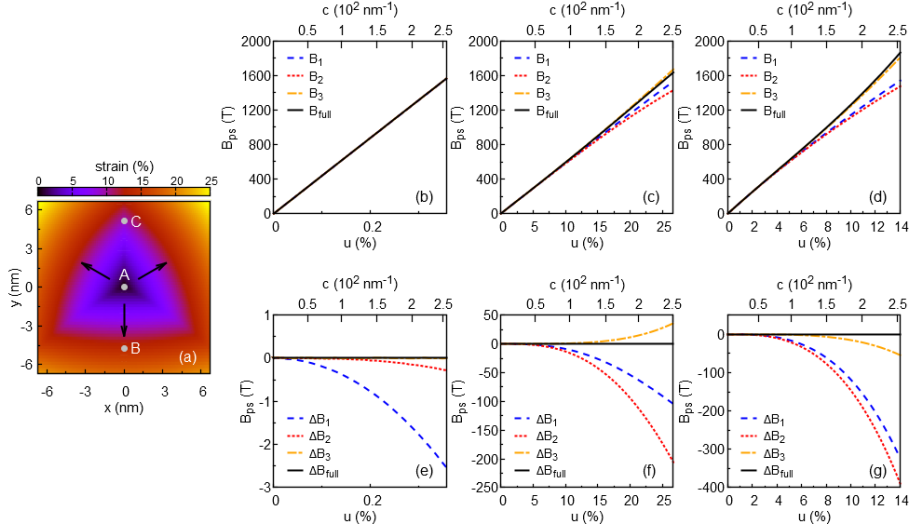


Figure 5: (a) Contour plot of the triaxial strain with three test points marked as A, B and C. The arrows indicate the strain directions. The parameters of the triaxial strain are the same as in Fig. 3. (b,c,d) The pseudo-magnetic field as a function of the strain at the three test points: (b) A, (c) B and (d) C. The field is calculated for different approximations of the hopping parameter from first to third order (B_1 to B_3 corresponds to $\delta r^{(1)}$ to $\delta r^{(3)}$), as well as the full solution (B_{full} for $\delta r^{(full)}$). (e,f,g) The differences of the pseudo-magnetic field approximations compared to the full expression ($\Delta B_i = B_i - B_{full}$) at the three test points: (e) A, (f) B and (g) C. In all cases the strain constant c is scaled from 0 to 0.025 nm^{-1} , as shown on the top x -axis. The resulting strain at the test point is shown on the bottom x -axis.

5. Conclusions

We investigated the pseudo magnetic field generated by strain using the tight-binding approximation. The hopping parameter and the deformation of the lattice vectors are expanded up to second order in the strain. The contribution of the different terms are compared with the full numerical solution for the pseudo magnetic field induced by a model triaxial strain.

For our numerical calculation a triaxial force is used to strain graphene and we obtained the pseudo magnetic field resulting from the different contributions resulting from different expansion terms and compared the results with the full solution. Numerical results for uniaxial strain clearly show that with applying strain the Fermi velocity is spatial dependent. We included the second order term in strain in the calculation of the pseudo magnetic field and showed that the first order strain is reasonably valid up to 15% strain and that the pseudo magnetic field is the same in all \mathbf{K} -points.

6. Acknowledgment

This work was supported by the Flemish Science Foundation (FWO-VI), the European Science Foundation (ESF) under the EUROCORES Program EuroGRAPHENE within the project CONGRAN and the Methusalem programme of the Flemish government.

References

- [1] K. S. Novoselov, A. K. Geim, S. V. Morozov, D. Jiang, M.I. Katsnelson, I. V. Grigorieva, S. V. Dubonos, and A. A. Firsov, *Nature (London)* **438**, 197 (2005).
- [2] Y. Zheng, Y. W. Tan, H. L. Stormer, and P. Kim, *Nature (London)* **438**, 201 (2005).
- [3] A. H. Castro Neto, F. Guinea, N. M. R. Peres, K. S. Novoselov, and A. K. Geim, *Rev. Mod. Phys.* **81**, 109 (2009).
- [4] C. Lee, X. Wei, J. W. Kysar, and J. Hone, *Science* **321**, 385 (2008).
- [5] V. M. Pereira, and A. H. Castro Neto, *Phys. Rev. Lett.* **103**, 046801 (2009).
- [6] F. Guinea, M. I. Katsnelson, and A. K. Geim, *Nat. Phys.* **6**, 30 (2010).
- [7] F. Guinea, A. K. Geim, M. I. Katsnelson, and K. S. Novoselov, *Phys. Rev. B* **81**, 035408 (2010).
- [8] F. Guinea, M. I. Katsnelson, and M. A. H. Vozmediano, *Phys. Rev. B* **77**, 075422 (2008).
- [9] M. Neek-Amal, and F. M. Peeters, *Phys. Rev. B* **85**, 195446 (2012); *ibid.* **85**, 195445 (2012).
- [10] M. Neek-Amal, L. Covaci, and F. M. Peeters, *Phys. Rev. B* **86**, 041405 (2012).
- [11] N. Levy, S. A. Burke, K. L. Meaker, M. Panlasigui, A. Zettl, F. Guinea, A. H. Castro Neto, and M. F. Crommie, *Science* **329**, 544 (2010).
- [12] T. Georgiou, L. Britnell, P. Blake, R. V. Gorbachev, A. Gholinia, A. K. Geim, C. Casiraghi, and K. S. Novoselov, *Appl. Phys. Lett.* **99**, 093103 (2011).
- [13] H. Suzuura and T. Ando, *Phys. Rev. B* **65**, 235412 (2002).
- [14] J. L. Mañes, *Phys. Rev. B* **76**, 045430 (2007).
- [15] A. L. Kitt, Vitor M. Pereira, Anna K. Swan, and Bennett B. Goldberg, *Phys. Rev. B* **85**, 115432 (2012).
- [16] A. L. Kitt, Vitor M. Pereira, Anna K. Swan, and Bennett B. Goldberg, *Phys. Rev. B* **87**, 159909(E) (2013).
- [17] F. D. Juan, M. Sturla, and M. A. H. Vozmediano, *Phys. Rev. Lett.* **108**, 227205 (2012).
- [18] F. D. Juan, Juan L. Mañes, and M. A. H. Vozmediano, *Phys. Rev. B* **87**, 165131 (2013).